Overview of NASA's Sentinel-6 Michael Freilich Satellite Mission

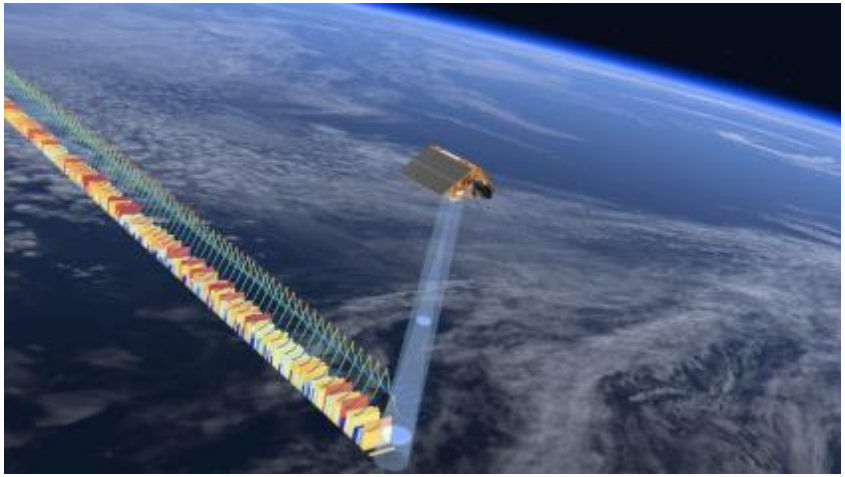

Phase 1 of 2 launched on November 21st 2020.

This satellite measures the sea level of more than 90% of the worlds oceans down to the centimeter.

Named after Michael Freilich, who was the director of NASA's Earth Science Division.

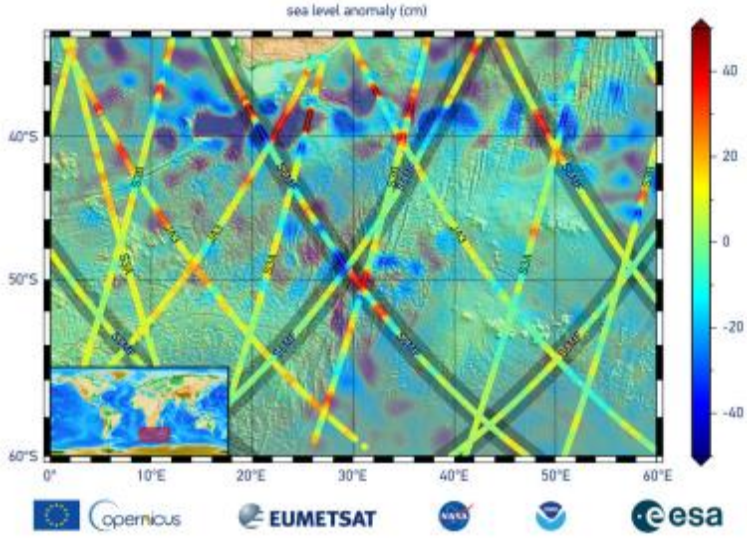

First data posted on December 10th

Satellite Instruments:
-Poseidon-4 SAR Radar Altimeter
- Advanced microwave radiometer for Climate (AMR-C)
- Global Navigation Satellite System - Radio Occultation (GNSS-RO)
- Doppler Orbitography and Radiopositioning Integrated by Satellite (DORIS)
- Laser Retroreflector Array (LRA)

CUSTOM DATA SCIENCE TOOL KIT FOR WIND AND GPS DATA

FINN BURMEISTER-MORTON

Introduction

The fields of data science and machine learning are critical to fully utilizing your scientific data. To simplify this process, an automated, flexible data science tool kit was built for data transformation, visualization, and modeling. This toolkit was used with a project involving complex wind and GPS data.

Methodology

Wind Data was automatically loaded, transformed, and graphed in just two lines of code

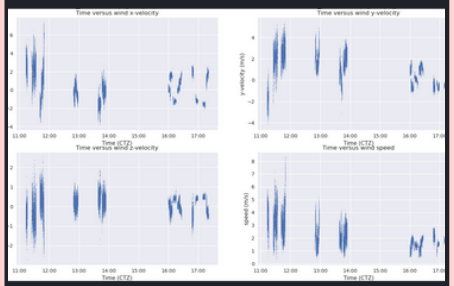

Methodology (con't)

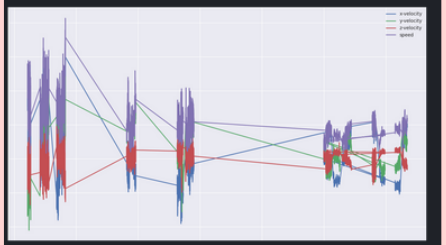

Completely changing the data's presentation style was accomplished in a few words

Methodology (con't)

Complex data types were seamlessly visualized

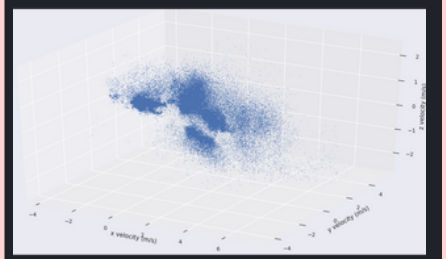

Conclusion

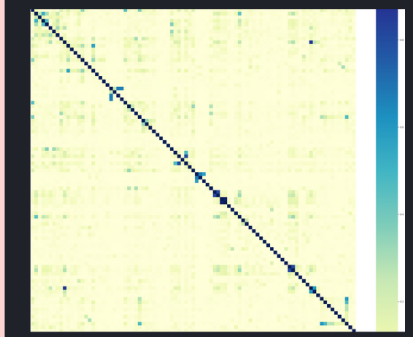

Automated and visualized the machine learning process from preprocessing to deployment

Evaluating Ice Production of Ross Ice Shelf and Terra Nova Bay Polynyas during 2019 using Sentinel-1 SAR Image and ICESat-2 data

[1]Elizabeth Hebel and [2]Dr. Hongjie Xie
1. University of Colorado Boulder, Boulder, Colorado 2.The University of Texas at San Antonio, San Antonio, TX

Research

- Polynyas are formed by wind blowing sea ice away from the ice shelf edge
- This area of open water allows more sea ice to form
- It's an important source of heat exchange, space for phytoplankton to get sunlight, and salt from brine rejection while the sea ice is forming.

Our study incorporates the use of ICESat-2 along with Sentinel-1 Synthetic Aperture Radar (SAR) to quantify the seasonal sea ice production for the Ross Sea Polynya, McMurdo Sound Polynya, and the Terra Nova Bay

Study Area

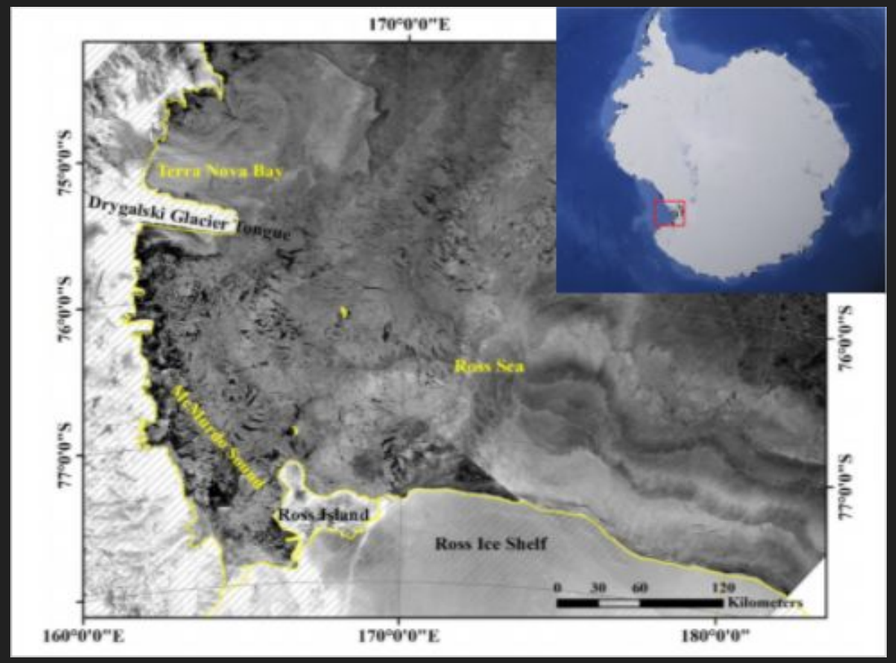

Our research looks at how wind events create 'Sea Ice Factories' in the Ross Sea and Terra Nova Bay in Antarctica

Method

- Sentinel-1 Synthetic Aperture Radar was collected to determine the duration, extent and frequency of polynya events for the study areas between the months of March and November 2019.
- The extent of each event was done manually.
- ICESat-2 ATL-10 was collected to determine sea ice freeboard through laser altimetry.

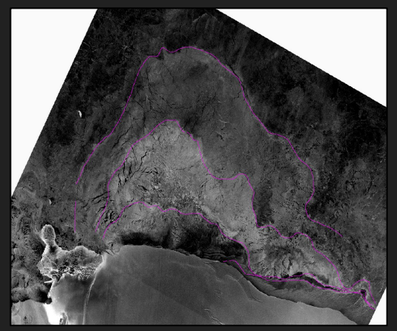

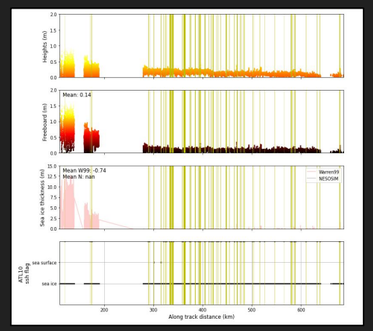

Results

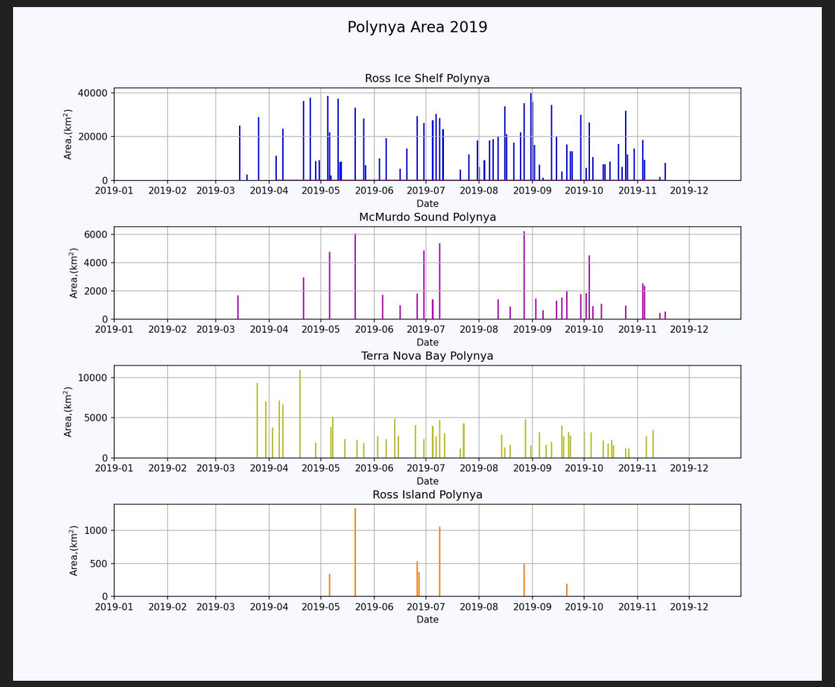

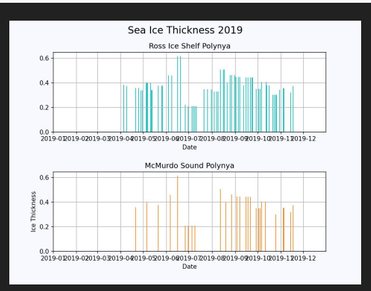

Further Research

Improvement to calculations that derive Freeboard to Ice Thickness when studying thinner Pancake Ice.

Cross-validation with AMSR2 Brightness Temperatures

Using LIDAR for Mapping Terrain

Abstract

LIDAR has become a popular tool to be used in robotics and it is being used in some autonomous cars that are on the roads today. In this case, the LIDAR sensor is going to be focused on mapping a terrain that is close to mars. This requires a sensor that is capable of getting data similar to a point cloud. Through my findings it is possible to map terrain using a LIDAR sensor and implementing a slam system would be useful for creating autonomous missions.

Mapping method

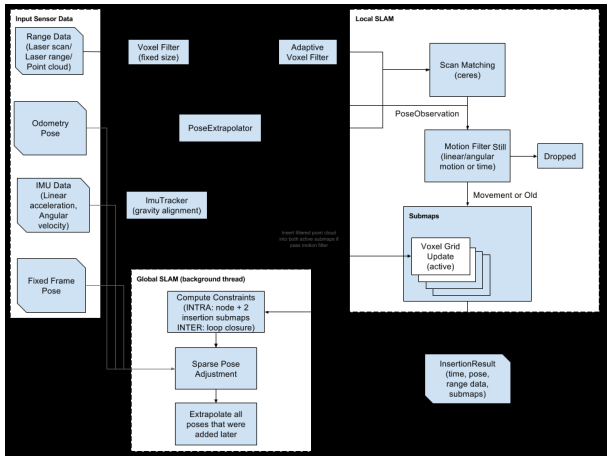

(1) Google cartographer's SLAM algorithm

- Grab data from the LIDAR and IMU. Then push them to the local SLAM
- If the global SLAM contains the local SLAM already don't insert it
- If there has been movement and the local slam is different insert into the global SLAM

Conclusion

- LIDAR can capture in various conditions which is useful to obtain an accurate map
- Point clouds are not always accurate and utilizing sensor fusion with our IMU(Inertial Measurement Unit) can help our map be a lot cleaner.
- Creating a self healing map could help make the system more time efficient
- Although Google Cartographer's algorithm is good, we can improve it by using continuous time SLAM.
- LIDAR and Stereo Vision have distinct differences but for mapping LIDAR might be the better choice.

LIDAR vs Stereo Vision

LIDAR and stereo vision have been two conflicting technologies and they both have their pros and cons.

LIDAR

- Point cloud data
- Work with bright light and dark shadows
- Relies heavily on moving mechanical parts

Stereo Vision (Visual Odometry)

- Grabs feature points and creates a 3d map
- Sees more of the scene
- Lightweight and easy to put in place

Continuous time

- Lines and edges in the right figure are cleaner and smoother

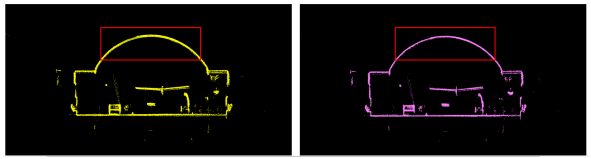

(2) LEFT-Orignial scan RIGHT-Cleaner lines with continuous time algorithmn

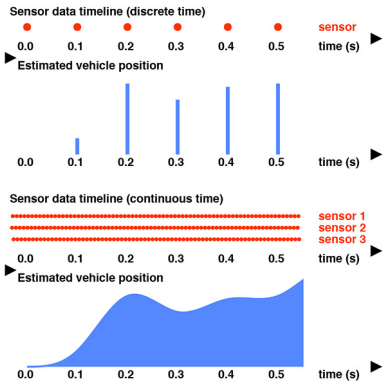

(1) Continuous time graphic

- Continuous time attempts to estimate the positions in between certain time points in the sensor's time out zones where it doesn't collect data. This allows the map to be overall cleaner.

Self Healing Map

- The system should be able to heal by itself which entails that it should be able to detect changes and only update the bigger map if it has changed at all to be more efficient.

Future Work

- Test LIDAR sensor mapping with the OS-1-16 LIDAR sensor.
- Implement the continuous time to the mapping algorithm.
- Figure out map compression methods to save space.
- Compare the use of LIDAR SLAM and Visual Odometry SLAM for exploring planets outside of our own.

References

https://www.wired.com/story/how-nasa-built-a-self-driving-car-for-its-next-mars-mission/
(1) https://ouster.com/blog/building-maps-using-google-cartographer-and-the-os1-lidar-sensor/
(2) https://www.researchgate.net/publication/313945676_IMPROVING_GOOGLE'S_CARTOGRAPHER_3D_MAPPING_BY_CONTINUOUS-TIME_SLAM
https://www.tegakari.net/en/2020/07/sp-slam-info/

Undergraduate MARS Rover Team

Zach Riddle
The University of Texas at San Antonio, San Antonio TX, 78249

Introduction

•Rovers are surface exploration vehicles equipped with an array of scientific instruments used to gather and interpret data from its deployed surroundings.

• In space exploration, NASA uses rovers to research Mars's surface and to find clues of past water activity.

• A suspension system known as the "Rocker-Bogie" enables NASA's Rovers to traverse the harsh environment found on Mars.

Objective

- To create a rover design capable of taking scientific measurements by integrating the planetary exploration abilities of Curiosity
- Overcome obstacles that can be found on the surface of Mars from environmental terrain to atmospheric conditions
- Explore possible ways to improve rover locomotion and enhance performance.

Methods

- 3D print the different parts of the rover based on the requirements of the rover and the physical properties of a variety of plastic filament.
- Test the different iterative rover designs on constructed tiles that reflect mars surface features in order to measure the designs performance.
- Conduct simulated analysis to test if the mechanical parts of the rover will fail or deform under applicable stress.

Results

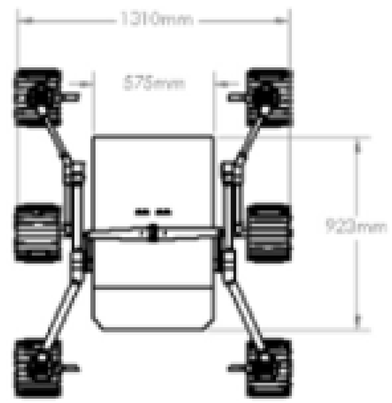

Figure 1: Top View of the Current Rover Design

Results - con't

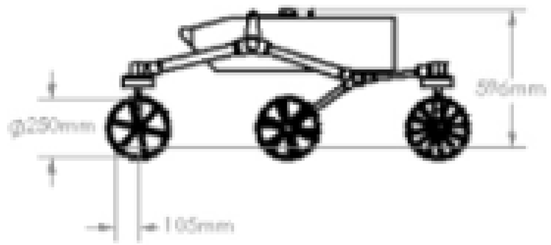

Figure 2: Side View of the Current Rover Design

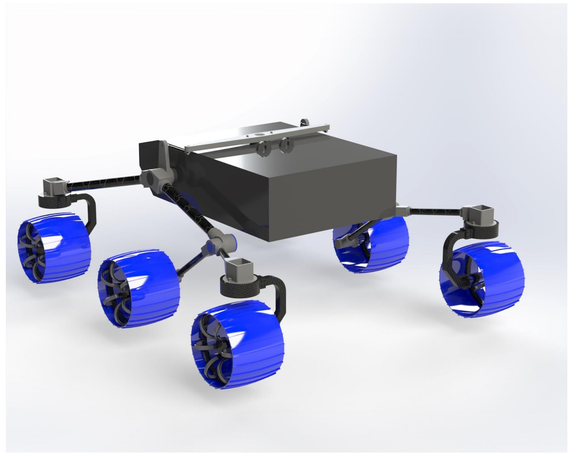

Figure 3: Rendered model of the Current Rover Design

Summary

- Created our first rover design, based off the rocker bogie suspension of the Curiosity rover, to be capable of traversing environmental obstacles that could be found on the surface of Mars.
- Currently in the process of 3D printing the different parts for assembly

Acknowledgments

NASA MIRO CAMEE

Laboratory of Turbulence, Sensing and Intelligence Systems

Dr. Kiran Bhaganagar

Dr. Patrick Benavidez

Logan Robinson, Brenda Carrillo, Wes Smithers, and Joshua Lee

USE OF UAV MULTIROTOR FOR ABL MEASUREMENTS AND PLUME STUDIES

Daniel Brun and Kiran Bhaganagar
Department of Mechanical Engineering, University of Texas, San Antonio (UTSA), TX,78249

Center for Advanced Measurements in Extreme Environments

Introduction

- The position of sensors in UAV is essential to obtain accurate data.
- It is required to study the aerodynamic of the propellers mounted on UAV.
- The average flight time of a UAV is of 20 – 30 minutes. The charging time of batteries is around 92 to 110 minutes.
- The collection of data on air with computers placed on the airframe would add weight to the UAV.
- Data collected size could be considered as big data.
- UAVs represent a risk when flown in populated areas.

Objectives

- Provide a longer flight-time for a DJI M600.
- Collect measurements and provide a real-time data feedback to monitor sensors.
- Increase safety factor when using UAV in populated areas.
- UGV measurements to collect data ground level.

Methods

- Wind velocity and temperature sensors are mounted on airframe of DJI M600
- A tethered system designed to provide power to DJI M600 and transmit real-time data
- Collect wind and velocity measurements at different heights
- Use UGV connected to tethered system to collect wind and temperature measurements at ground level

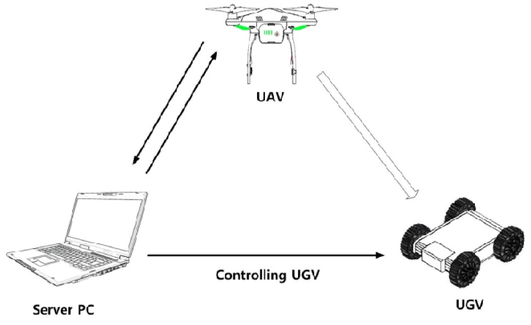

Results

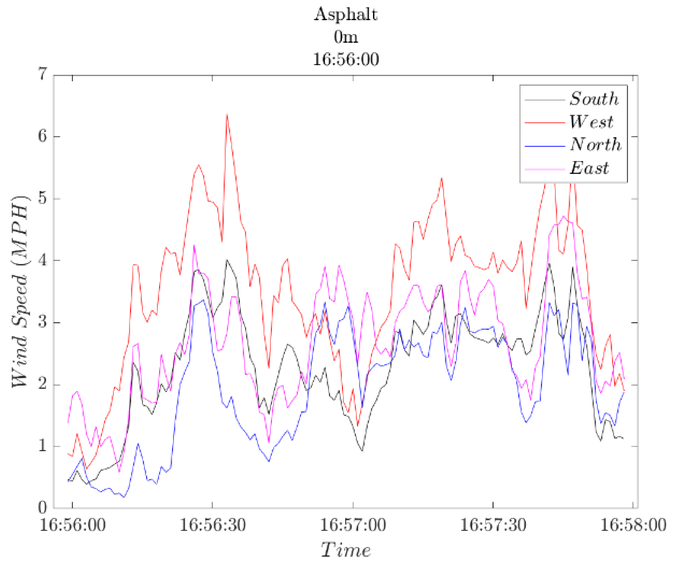

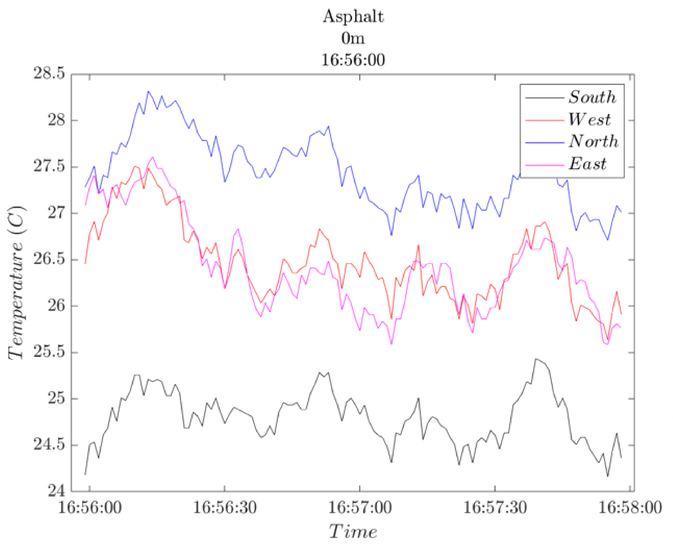

Conclusions

- Overall goal of the proposed study is to use UAV to monitor plumes in the atmosphere.
- Velocity indicates higher readings from the sensor aimed to the direction of the wind measured.
- Function in the graphs showing the temperature and velocity change during time is similar for the four sensors on the multirotor.
- Temperature is seen to have its highest value from the sensors aimed to the opposite side of the wind direction
- An upgraded tethered system would be developed to introduce flight at different heights
- Sensors must be upgraded for more accurate data collection

Acknowledgements

NASA MIRO CAMEE

Laboratory of Turbulence, Sensing & Intelligence Systems, UTSA.

Diaphragm Testing for UTSA Mach 7 Ludwieg Tube

Problem Statement

Determine the thickness required for a diaphragm to burst between 1380kPathe range of 345kPa to at room temperature and have fragment-free flow.

Diaphragm Manufacturing

Aluminum Foil Diaphragm

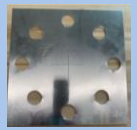

3105 -Aluminum Diaphragm

Experimental Set-up

UTSA Mach 7 Ludwieg Tube Wind Tunnel

Schlieren Z-Pattern Set-up

High-pressure components shown in red were used for testing. Schlieren Z-pattern configuration used to capture image flow.

Results

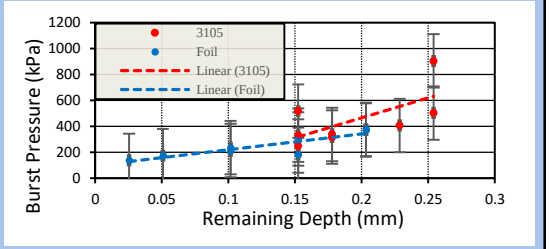

Rupture Data

Fully-Petaled Rupture

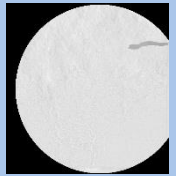

Fragment Caught by Schlieren

Fragmented Rupture

Matt Garcia & Christopher S. Combs

Work Sponsored in part by NASA grant 80NSSC19M0194
and AFOSR grant/contract FA9550-20-1-0190

Modal Analysis of Shock-Wave/Boundary-Layer Interactions

Introduction

Demand for hypersonic flight vehicles for applications in space exploration, defense, and commercial aviation.

NASA – X-15A (2014)

The Aviationist – damage to X-15A (2017)

Experimental Method

- Performed in NASA Langley Mach 6 tunnel
- Schlieren Visualization employed
- Flat plate and cylinder model

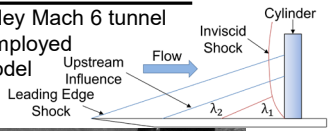

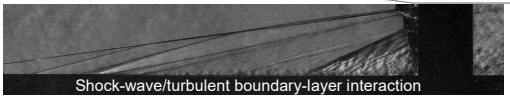

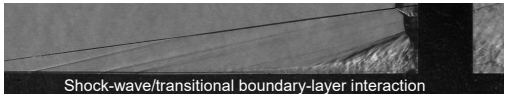

Results

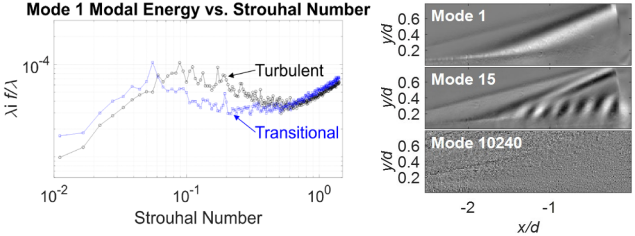

Future Work

Perform similar experiments with different geometries and surface roughness at UTSA.

Acknowledgements

NASA grant 80NSSC19M0194, ONR award number N00014-15-2269, AFOSR award number FA9550-20-1-0190, NASA LaRC (HTP, TTT, & AETC projects)

Estimation of Supraglacial Lake Depth On Antarctica Using ICESat-2

Introduction:

- Supraglacial lakes are observed in the ablation zones of Antarctica during the summer months.

- The role of surface water plays an important role on the stability of ice shelf.

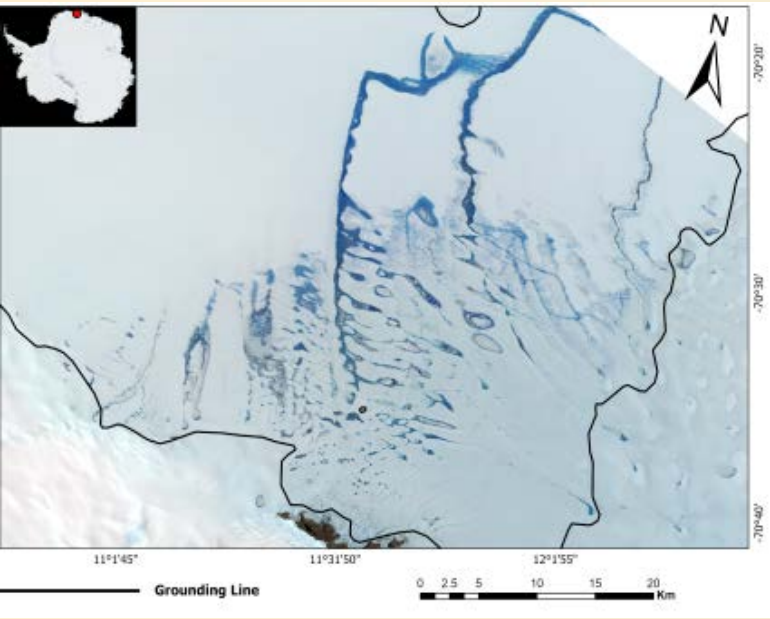

Fig.1 A map of study area. The base image is Landsat-8 acquired on 25th January 2019

Study Area:

- The Nivlisen Ice Shelf (70.3 S, 11.3 E) is situated in Dronning Maud Land, East Antarctica, between the Vigrid and Lazarev ice shelves.

Data and Methodology:

- Laser altimetry data from the Ice, Cloud, and land Elevation Satellite-2 (ICESat-2).

- ATL03 product:

Fair et al.,2020

$h_{sfc} - (1.8)\ \sigma_{sfc} \leq h_{btm} \leq h_{sfc} - (0.75)\ \sigma_{sfc}$

Where,

h_{sfc}= height of lake surface

σ_{sfc}=standard deviation of lake surface photons

h_{btm}= height of lake bottom

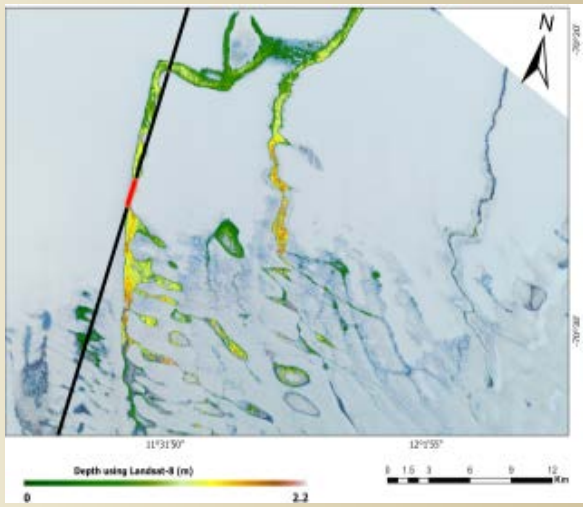

Fig.2 Depth estimation from Landsat-8 (Dell at al.,2020)

Results:

- **Mean Depth (m):**

ICESat-2	Landsat-8
1.77 ± 0.23	1.21 ± 0.17

- The difference between both the results is 0.56 m.

- Future work involves comparison with field data.

Application of Google Earth Engine (GEE) for automated tracking of iceberg B43 in the Southern Ocean

Center for Advanced Measurements in Extreme Environments

INTRODUCTION

[1] Iceberg B43

- Calved from Thwaites glaciers in the Amundsen Sea (April 2017)
- Broken in the Ross Sea (March 2020)
- Scientific importance of tracking icebergs: indicator of ocean current, influence on sea ice and ecosystems

[2] Sentinel-1 SAR data

- Useful data for monitoring icebergs: available for any weather conditions and any time
- Temporal resolution: < 2-3 days
- Spatial resolution: 10 m , 25 m, 40 m
- Free (accessible via GEE)

[3] Google Earth Engine (GEE)

- Cloud-based remote sensing data processing platform: Data storage + computing power
- Have NOT been actively used for monitoring of iceberg drift

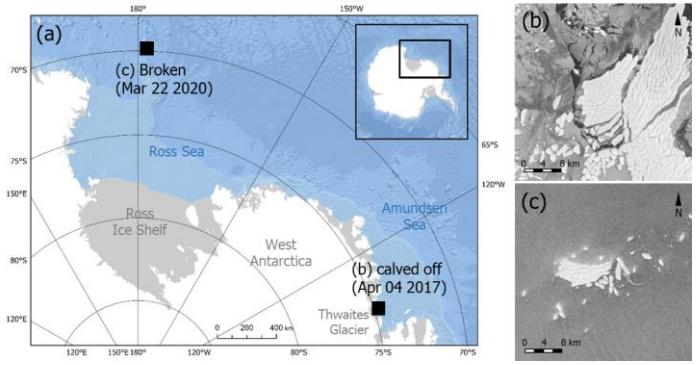

METHOD

[1] Detection of icebergs

- SNIC image segmentation + brightness ratio

[2] Tracking of the target iceberg

- Centroid distance histogram

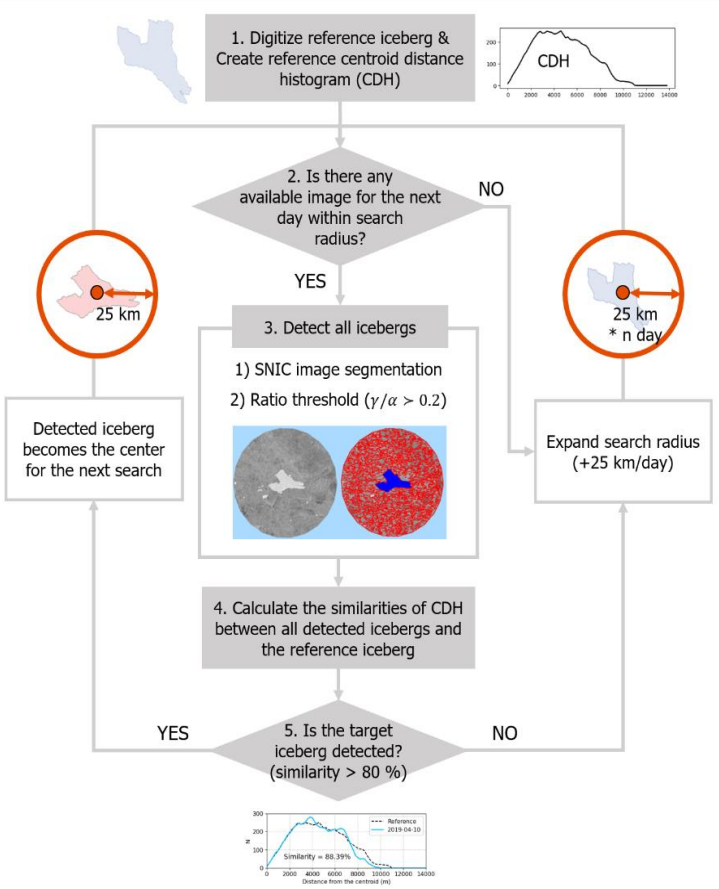

RESULTS

- Entire trajectory & drift speed of the iceberg

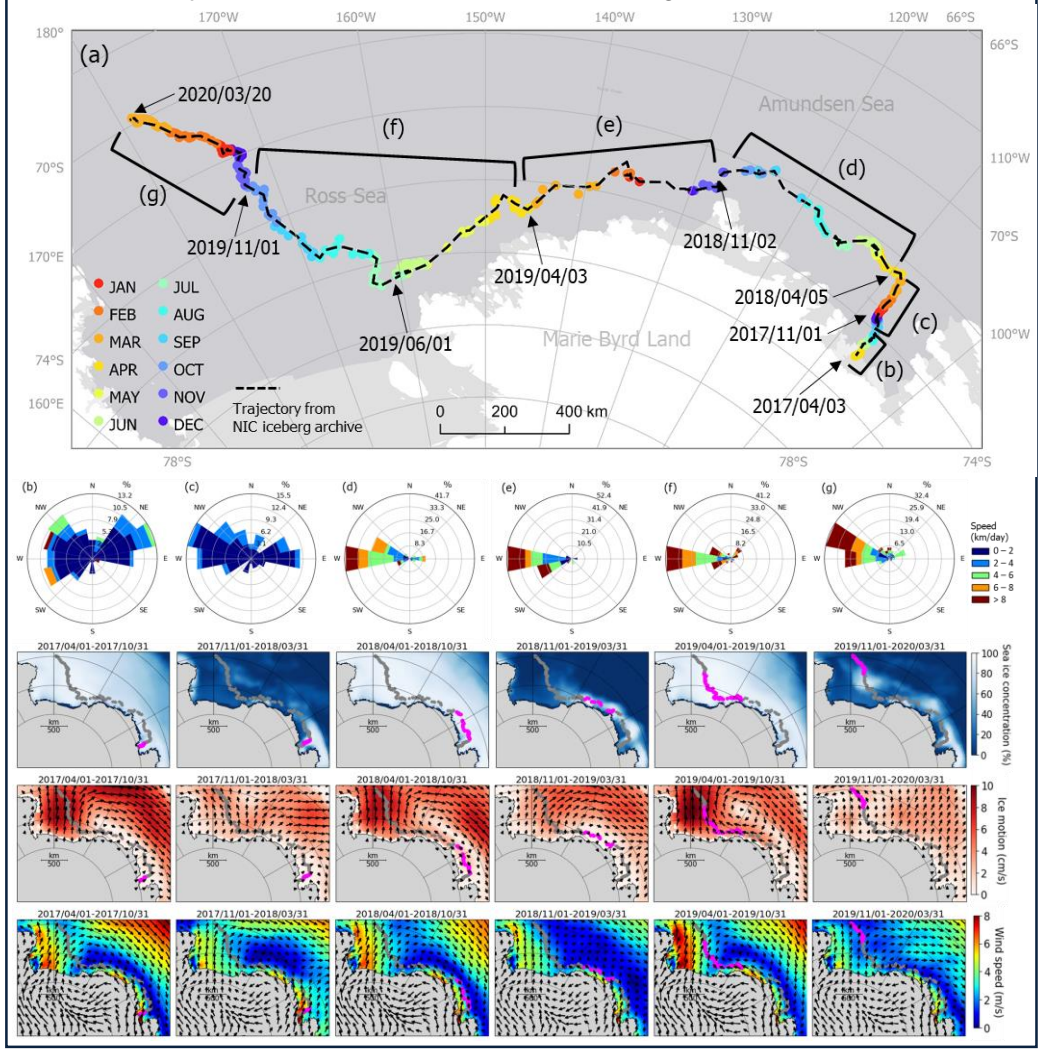

High-Speed Data Acquisition Triggering System for Hypersonic Wind Tunnel Applications

Introduction

Hypersonic wind tunnel applications require high-speed triggering modules for DAQ systems

Experimental Method

Performed in UTSA Hypersonics Lab
Testing for circuit development
Reliability and repeatability testing

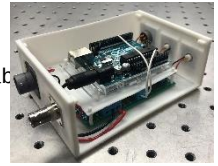

Completed Triggering Module

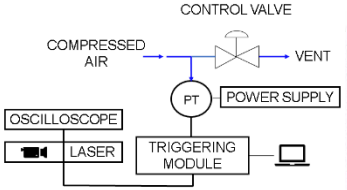

Testing configuration

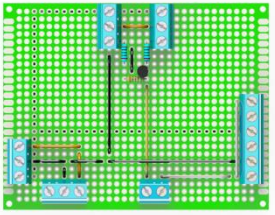

Low pass filter circuit

Results

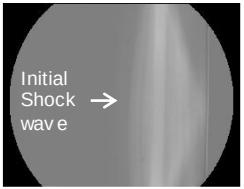

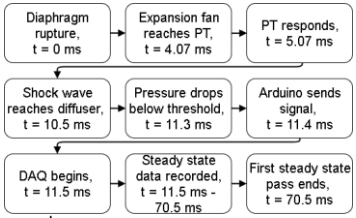

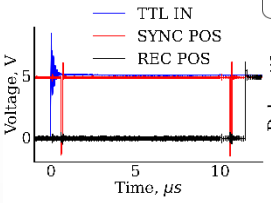

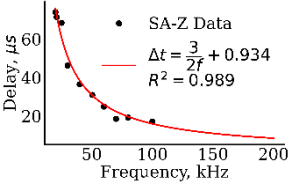

Triggering Pressure Drop: 47.36 kPa (6.87 psi) ± 5.93 kPa (0.86 psi)

Future Work

ESP-32 microcontroller
Data file size optimization

Processing Glider-based Ocean Velocity Observations

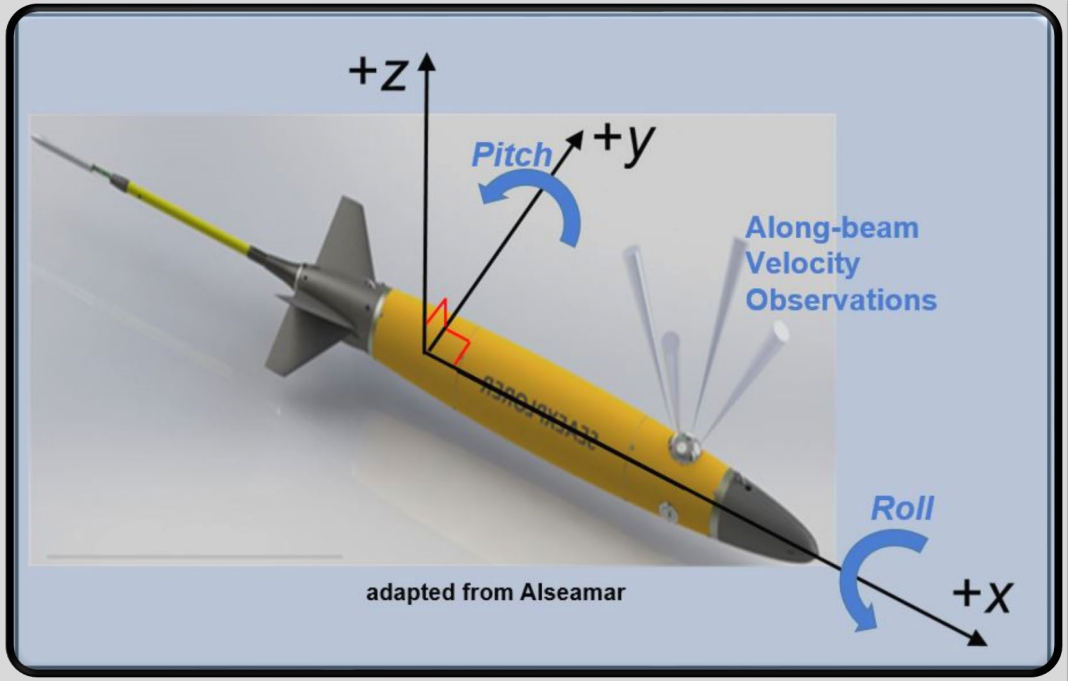

$$U_{adcp}(z,t) = \underbrace{U_{barotropic} + U_{baroclinic}(z)}_{\text{Absolute Ocean Velocity}} - U_{glider}(z,t)$$

adapted from Visbeck (2002)

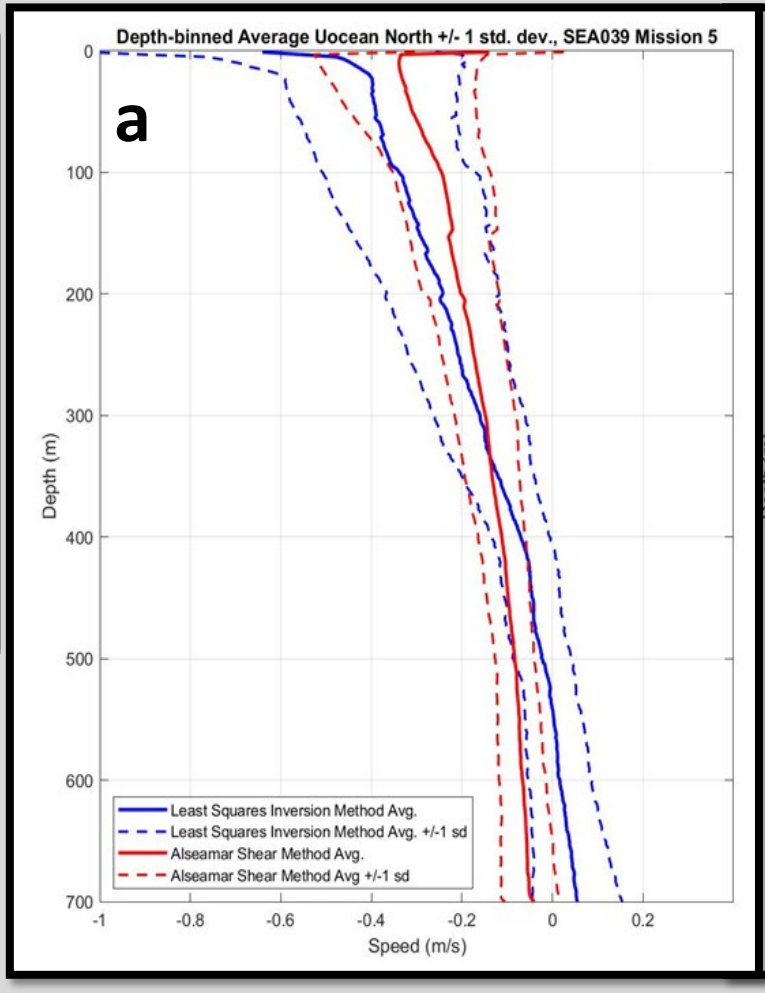

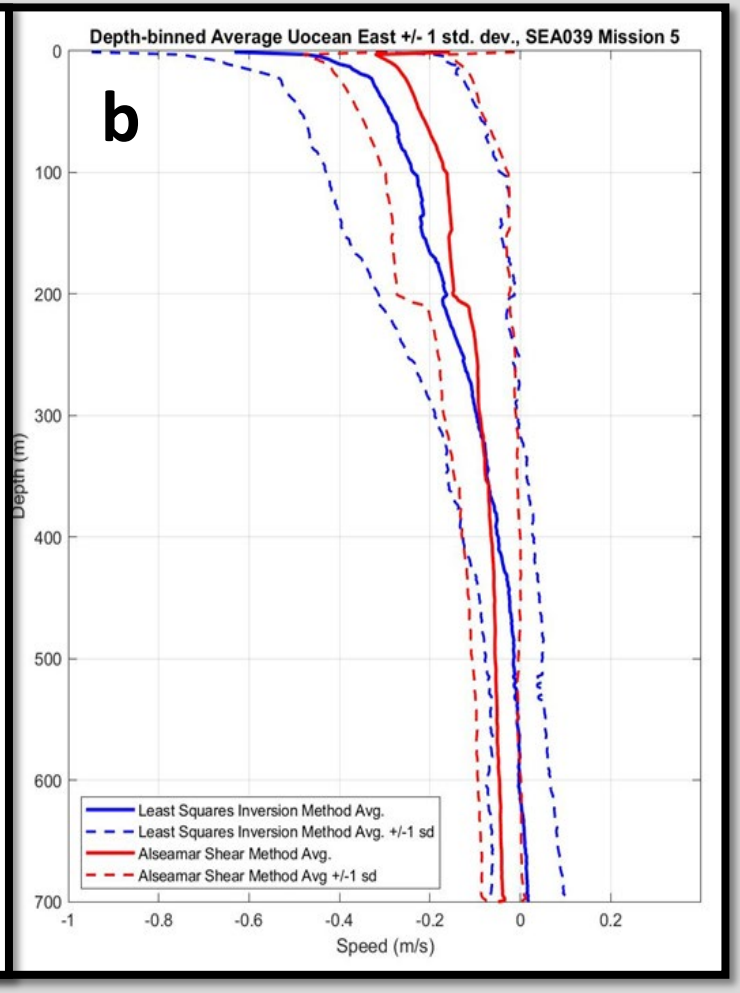

UTSA K. Mendiondo[1], A. Mestas-Nuñez[1], O. de Fommervault[2], H. Xie[1] [1] NASA MIRO CAMEE, Texas, USA [2] Alseamar-Alcen, Rousset, France

Determination of Large Hailstone Growth Using Stable Isotope

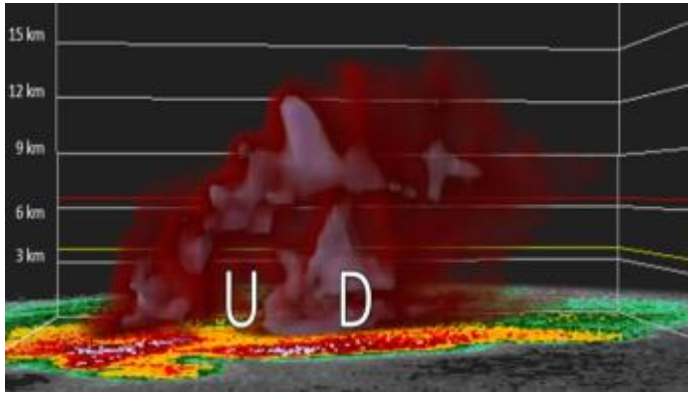

Figure 1, Del Rio Hailstorm 04/11/20, 3D model hail track 5.4 to 12.4 km. Nick Hampshire, NOAA

Hail causes significant damage to agriculture and property. San Antonio event on 12 April 2016 caused $1.4 billion in damage. "Car lots are magnets for large hail events" (Dr. Ackley).

Initial formation in supercell thunderstorms, Cumulonimbus clouds.

Hailstones accrete ice in an "onion" like fashion from a nucleus.

Small ice crystals form at lower temperatures than large crystals.

Many times hailstorms spontaneously form, their location and duration in many cases are unknown.

Collection of hailstones within thunderstorms is nearly impossible.

Research is important to better understand; origination mechanisms, formation temperature and flow paths of hailstones.

Outcomes from our research will aid in prediction, radar truthing and ground truthing.

Future research areas: water chemistry analysis, aerodynamics of hail and origination (nucleus) development.

Figure 2, Thin section.

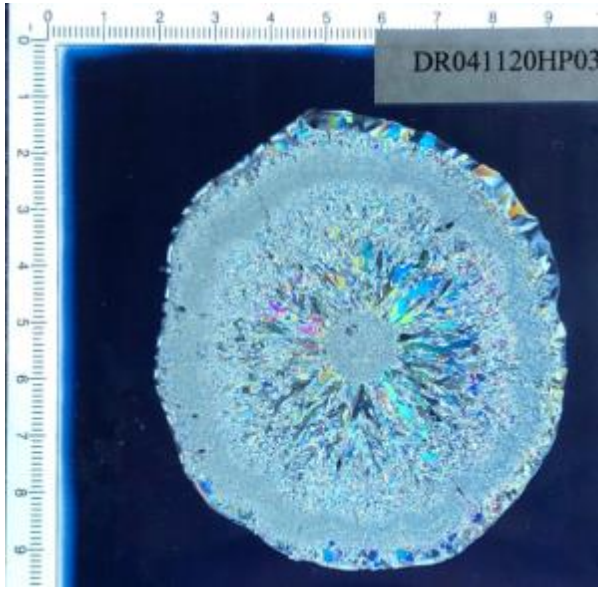

Figure 3, Thin Section Cross Polarized Light

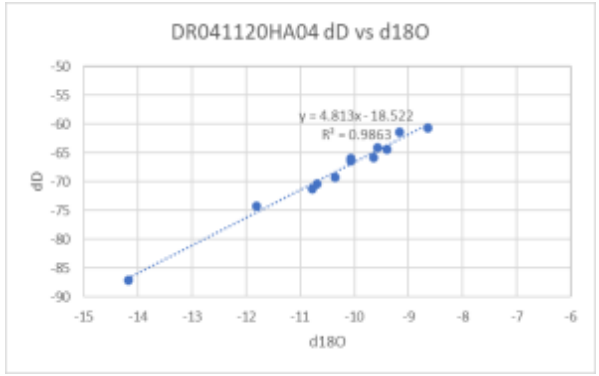

Figure 4, GMWL $\delta D = 8\delta^{18}O + 10$ (Craig 1961)

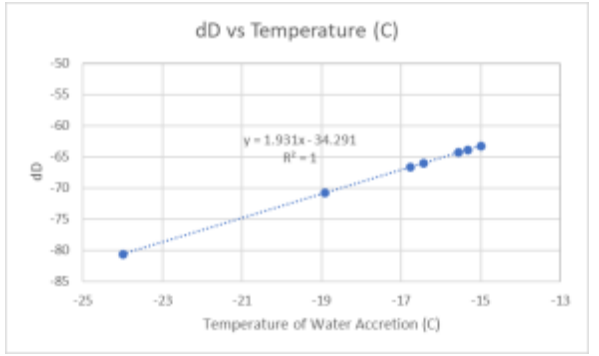

Figure 5, dD to determine Ice Temperature Accretion

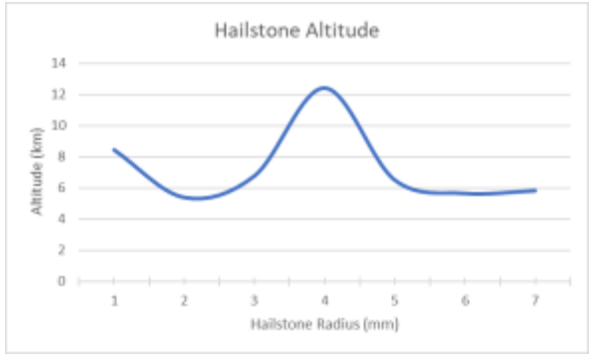

Figure 6, Altitude of Formation from Hailstone Temperature.

2021 CAMEE STUDENT RESEARCH SPRING SHOWCASE

Jesse Slaten & Kiran Bhaganagar[1]

[1]University of Texas at San Antonio

Buoyancy Driven Plumes in the Atmosphere/Environment

- Turbulent Plumes are a special class of flows that occur in a wide variety of geophysical phenomena with an equally large range of scales (from thermal vents in the ocean to wildland fires.)

Our problem is in the understanding of the unsteady evolution of entrainment E of these flows and there impact on turbulence mixing and other properties.

Figure 1: Ken Watson / kenwatson.net

Entrainment

Why even is this of interest?

Previous studies use the Entrainment Hypothesis which relates the mean inflow velocity u across the edge of a turbulent flow to a time averaged mean axial-velocity (centerline) by some dimensionless variable α_E. Usually assumed to be $\alpha_E = 0.16$ for pure buoyancy driven plumes.

$$\alpha_E u = w$$

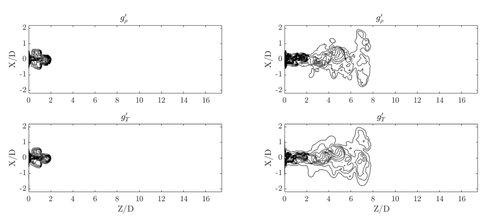

Figure 2: Time Evolution of Heated Gas Release (Helium)

Results

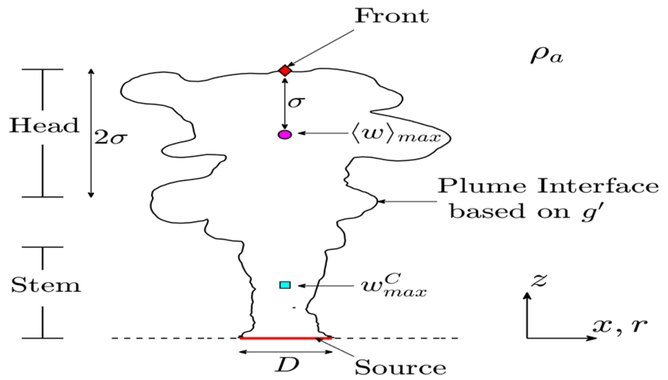

Fig. 3: Schematic of Plume

Our group has developed to formalize this unsteady entrainment based off key characteristics of the plume variables[1].

$$E = \frac{V(t_2) - V(t_1)}{W_f dt A_{\text{neck}}} \tag{1}$$

The question then arises how do certain characteristics variables such as

$$g'_T = \frac{T - T_{\text{amb}}}{T_{\text{amb}}} g \tag{2}$$

affect the plume growth and spread? Here we have a case study of 6 plumes (3 Helium releases and 3 case of heated air) and study the entrainment.

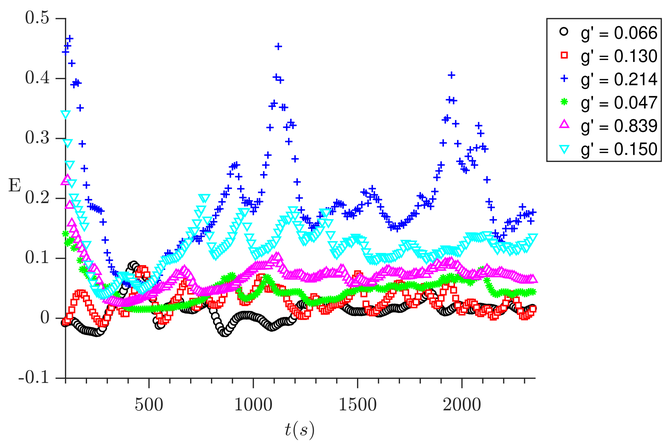

Fig. 4: Instantaneous entrainment evolution for 6 heated buoyancy driven plumes. Cases 1 - 3 : Helium. Cases 4-6: Heated Air (Thermal).

Scaling Parameters

Question: Does it scale with Re or Fr ?

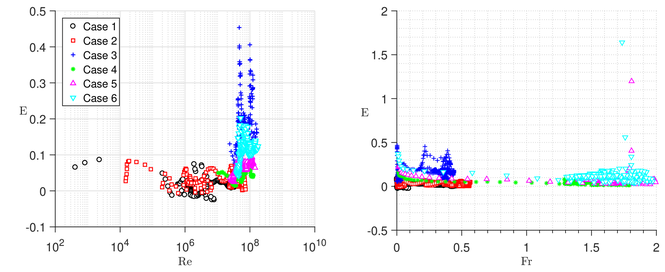

Fig. 5: A: Entrainment vs. log scaled local Reynolds number.

B Entrainment vs local Froudes number.

Comparisons

Case	Gas	$H_0[kms^{-1}]$	$g'_T[ms^{-2}]$	$\theta[k]$	Re_{w_c}	Fr_{w_c}	$\overline{E}$	$W_c max[ms^{-1}]$
1	Helium	0.5	0.0658	2.0113	3.3594e+07	0.1178	0.0801	1.0371
2	Helium	1.0	0.1296	3.9632	5.1397e+07	0.1908	0.1551	1.6795
3	Helium	2.0	0.2139	6.5412	7.5673e+07	0.5339	0.19591	4.7005
4	Air	0.5	0.0466	1.4255	5.6934e+07	0.7826	0.0657	5.477
5	Air	1.0	0.0839	2.5656	6.4171e+07	0.8775	0.0961	7.7261
6	Air	2.0	0.1496	4.5743	8.6342e+07	1.1654	0.1595	10.2604

Conclusions/Takeaways

- Without prior knowledge of this unsteady entrainment coefficient current models as well missing the mixing taking place which is important for control, forecasting and understanding the physics.
- Further study on this entrainment is in how it affects the turbulent kinetic energy (TKE) of these flows, and on more robust environments such as stratification (stable/unstable) within a planetary boundary layer.
- Future work to reveal answers to wildland fire plumes mixing and entrainment proccees.

References

[1] Kiran Bhaganagar and Sudheer R. Bhimireddy. “Numerical investigation of starting turbulent buoyant plumes released in neutral atmosphere”. en. In: *Journal of Fluid Mechanics* 900 (Oct. 2020), A32. ISSN: 0022-1120, 1469-7645. DOI: 10.1017/jfm.2020.474. URL: https://www.cambridge.org/core/product/identifier/S0022112020004747/type/journal_article (visited on 01/28/2021).

Comparisons of Geostrophic Current Observations from Buoyancy Gliders and OSCAR Data

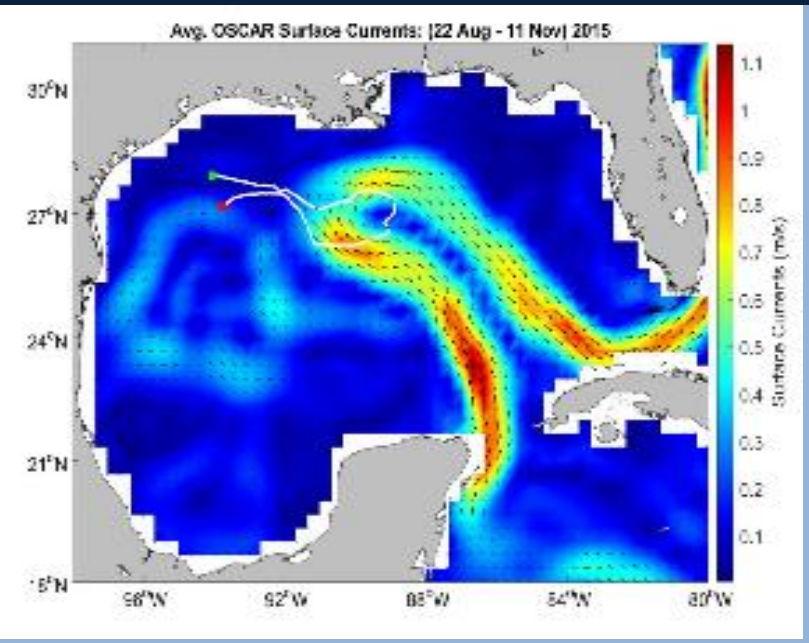

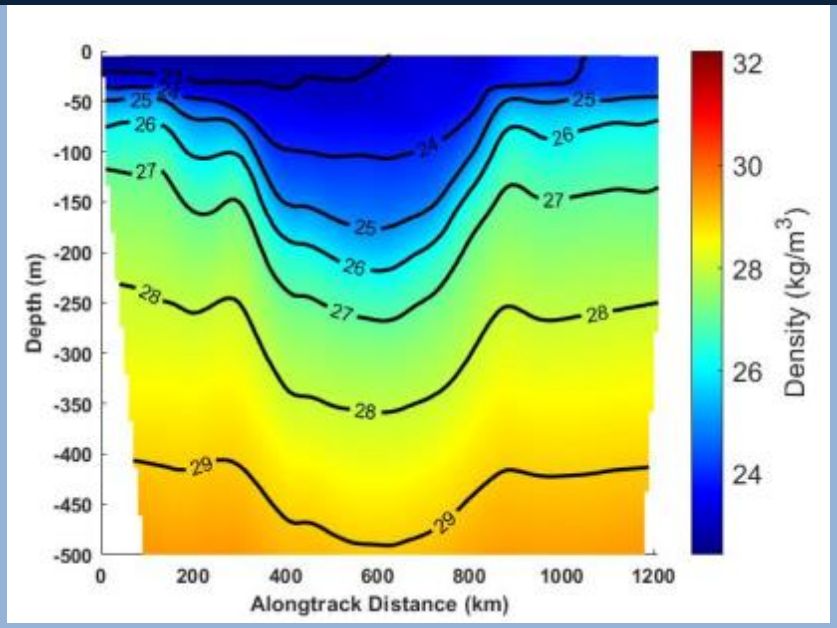

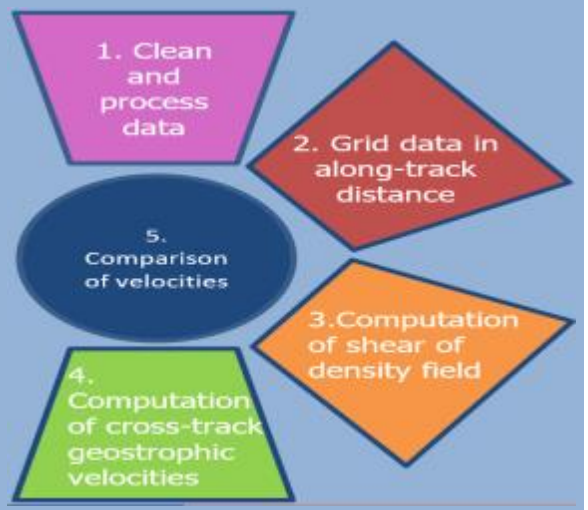

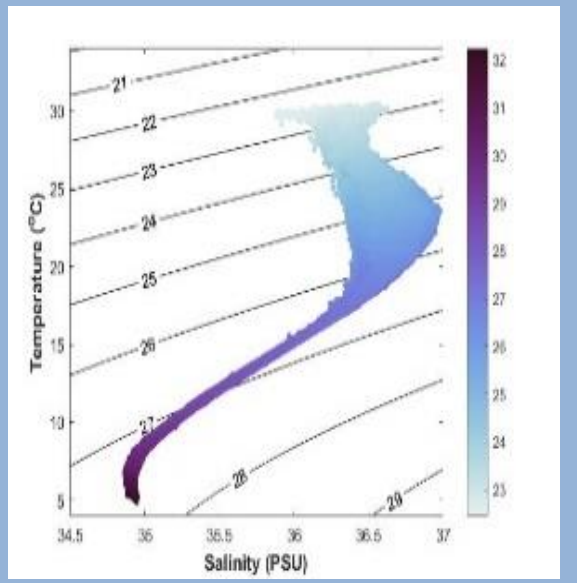

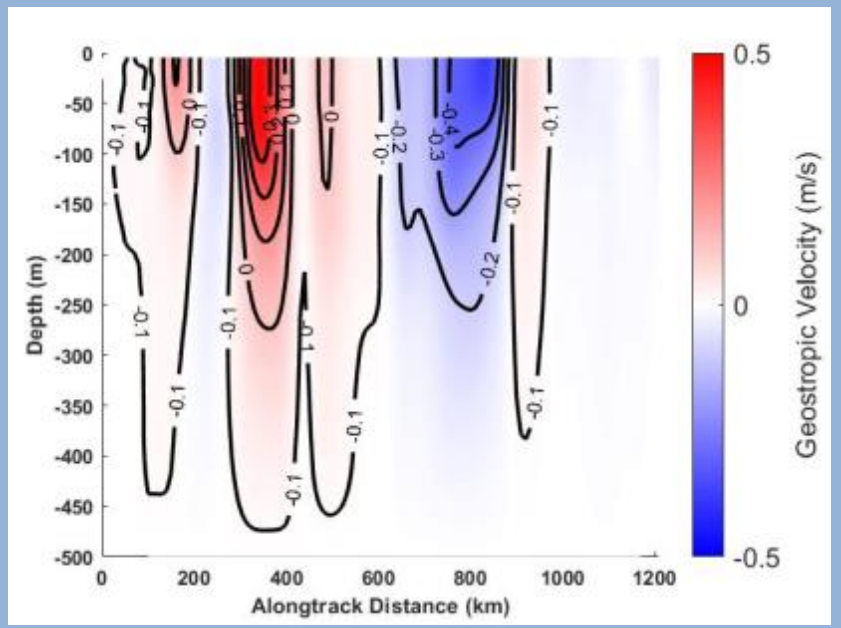

THE FOUR STAGE DEVELOPMENT OF STARTING TURBULENT BUOYANT PLUMES

Thanh Tran and Kiran Bhaganagar
Department of Mechanical Engineering, University of Texas, San Antonio (UTSA), TX,78249

Center for Advanced Measurements in Extreme Environments

Abstract

Turbulent heated and buoyant plumes have important applications in the atmosphere such as wildland fire plumes, volcanic plumes, and chemical plumes. Data from Weather Research Forecast model coupled with Large eddy simulation (WRF-bLES) with a two-way feedback between the buoyant plume and the atmosphere developed by UTSA team has been used. Five consisting of heavy gases (i) carbon dioxide and (ii) sulfur dioxide, and light, buoyant gases, (i) helium, (ii) ammonia, and (iii) heated air, were released into ambient still atmosphere from a circular source at the bottom of the domain. The simulations of axisymmetric plume were performed at high Reynolds number of 108. The first stage is the plume acceleration stage, the second stage corresponds to formation of head of the plume that grows spatially. Third stage is when the plume head is fully formed and the flow transitions to a quasi-steady state behavior. The final stage is the fully developed plume which had reached maximum height and spreads out radially at the top.

Introduction (Background)

Wildland fire (WF) had been one of biggest natural disaster that have a significant impact on air quality, climate and human safety. One phenomenal fluid dynamics characteristic of the WFs is the presence large fire whirls created by turbulent plumes rising into the atmosphere (Church, Snow & Dessens, 1980).These large fire whirls increase the WF spreading range significantly resulting in a complex fire behavior that is difficult to predict (Forthofer, Jason & Scott 2011).

In this study, turbulent thermal and buoyant plumes generated from a large-scale simulation by Weather Research Forecast model coupled with Large eddy simulation (WRF-bLES) are analyzed. WRF-bLES is an inhouse tool developed to simulate the two-way dynamic interactions between the atmosphere and the plume. (Bhaganagar & BhimiReddy, 2020; BhimiReddy & Bhaganagar, 2018). The analysis has been conducted for five different source conditions obtained by varying the gas released at the source. The cases are classified as release of (A) heavier than ambient source fluid with So2 and Co2 gases, B) lighter source fluid with He and NH3 and heated air gases. The focus of this study is to understand the stages of the development of a starting, turbulent, axisymmetric buoyant plume released from a circular source, and to quantify the plume characteristics through flow visualization techniques.

Purpose (Objective, Aim, Goal)

The purpose of the study is to conduct an analysis of the turbulence structures to understand the stages of the development of the turbulent plumes. The identification of the four-stage development of the plume has important significance to characterize realistic plumes and to quantify the extent of mixing at each of these stages.

Methods

- The physical domain of simulation is 7km (height) x 1.8km x 1.8km (horizontal direction). The diameter of the circular source (D) of the released gas 400 meters.
- The mesh resolution is 40 meters in the horizontal direction, and 10 meters in the vertical direction. The ambient condition is still air maintained at a constant temperature of 300K.
- The buoyancy generated at the source is characterized using difference in the by the density difference between the gas at the source and the ambience and the temperature difference between the gas at the source and the ambience.
- For each data case u, v, w velocity data were imported and used to calculate λ2 vortex criteria.
- The details of the five cases analyzed in this study are shown in Table 1. There are two inputs for the simulation: initial gas constant, R0, and constant surface heat flux, H0, shows in table 1. H0 is the constant heat flux of the surface diameter D at the bottom boundary.

	Heavy gas		Lighter gas		
	Case 1	Case 2	Case 3	Case 4	Case 5
Gas released	So_2	Co_2	He	NH_3	Thermal Plume
R_0 (J/kg·k)	129.78	188.92	2077.1	488.21	287.00
H_0 (kms^{-1})	2.5	5.0	2.0	2.5	0.5
$g'_{T0}(ms^{-2})$	0.1962	0.5029	0.2006	0.1850	0.0820
$g'_{\rho 0}(ms^{-2})$	-11.24	-6.04	8.49	2.92	0.00
$W_{fs}(s^{-1})$	0.0025	0.0054	0.0040	0.0060	0.0180
$W_{cm}(ms^{-1})$	1.760	12.710	4.700	14.320	5.760
z_{wcm}	2.275	1.675	2.000	3.700	1.625
l_{wcm}	0.900	0.600	0.900	1.100	0.6292
Re_{wcm}	4.04e7	1.94e8	1.08e8	4.01e8	9.23e7
$w_b(s^{-1})$	8.8589	14.183	8.9577	8.6023	5.7271
Fr	0.1988	0.8962	0.5248	1.6649	1.0049

TABLE 1. Initial conditions and dimensionless number for simulated plume cases.

Results

Figure 1 shows the front velocity plot of the five cases which are So2, Co2, He, NH3, and thermal plume (Fig. 1a, 1b, 1c, 1d, and 1e respectively). The x-axis of the plot is the instantaneous frontal velocity of the plume, and y axis is the time in seconds from the initial release time. Figure 2 shows λ2 Isosurface of the plume temperature during all four stages.

Results - con't

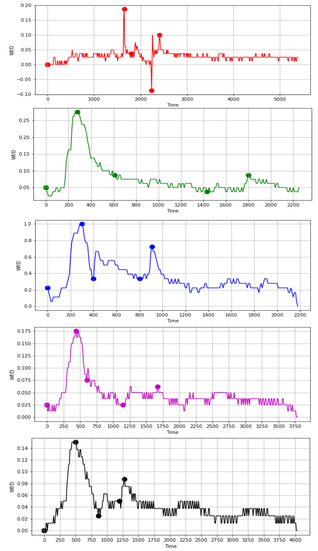

a) Case1: So_2 *front velocity.* *(R_0: 129.78 J/kg·k, H_0: 2.5* kms^{-1}*)*

b) Case2: Co_2 *front velocity.* *(R_0: 188.92 J/kg·k, H_0: 5* kms^{-1}*)*

c) Case3: He front velocity. (R0: 2077.1 J/kg·k, H0: 2 kms-1)

d) Case 4: NH3 front velocity. (R0: 488.21 J/kg·k, H0: 2.5 kms-1)

e) Case5: Thermal Plume front velocity. (R0: 287.00 J/kg·k, H0:0.5 kms-1)

Figure 1. Front Velocity of Five Cases (1-5). After an initial transience, the plume goes through an acceleration stage and reaches a peak velocity. The time taken to reach the peak velocity varies with each case.

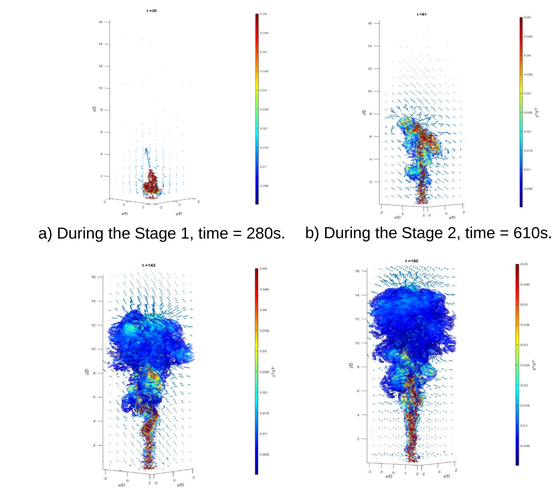

a) During the Stage 1, time = 280s. b) During the Stage 2, time = 610s.

c) During the Stage 3, time = 1430s. d) During the Stage 4, time = 1800s.

Figure 2. The λ2 Isosurface of the plume temperature difference overlayed on velocity vectors during stage 1-4 for case 3 (Co2) is shown.

Conclusions

- **First stage** is defined as the initial stage of the plume during which the plume accelerates from an initial state and reaches a maximum front velocity. This is the acceleration stage. During this stage, the turbulent plume raises axially without significant radial expansion.
- **Second stage** is defined as the duration during which the plume head forms. The formation of the head corresponds to resulting deceleration of the plume front. During this stage, a well-defined circular vortex structures are evident.
- **Third stage** is defined as the stage when the plume head is fully formed and the flow transitions to a quasi-steady-state behavior. Head of plume is fully formed.
- **Four stage** is the fully developed plume which had reached its maximum height and it spreads out radially at the top.
- The results have demonstrated that all five cases, the turbulent plumes exhibit universal characteristics, and the development of the starting plumes occurs in four characteristic stages. The identification of the four-stage development of the plume has important significance to characterize realistic plumes and to quantify the extent of mixing at each of these stages. The work is an important step in not only the fundamental fluid dynamics of plumes but also in predicting and forecasting the plume trajectory of smoke, wildland fire or volcanic plumes.

References

1. Bhaganagar, K., & Bhimireddy, S. (2020). Numerical investigation of starting turbulent buoyant plumes released in neutral atmosphere. Journal of Fluid Mechanics, 900, A32. doi:10.1017/jfm.2020.474.
2. Bhimireddy, Sudheer & Bhaganagar, Kiran, Short-term passive tracer plume dispersion in convective boundary layer using a high-resolution WRF-ARW model, *Atmospheric Pollution Research, 9:901-911, 2018.*
3. Forthofer, Jason & Goodrick, Scott. (2011). Review of Vortices in Wildland Fire. Hindawi Publishing Corporation Journal of Combustion. 14. 10.1155/2011/984363.
4. Jinhee Jeong, Fazle Hussain, 1995 On the identification of a vortex J. Fluid Mech., pp.69-94.

Acknowledgements

Funding for this study is provided by NASA MIRO CAMEE. Experiment was conducted at the Laboratory of Turbulence, Sensing & Intelligence Systems, UTSA.

Arctic Cyclones and Their Interactions with Declining Sea Ice

Elina Valkonen [1,2], Elizabeth Cassano,[1] And John J Cassano,[1,2]

1. National Snow and Ice Data Center, University of Colorado Boulder,
2. ATOC, Department of Atmospheric and Oceanic Sciences, University of Colorado Boulder

Background

- The Arctic sea is thinning rapidly, and the full responses to the changing polar climate is still unknown
- The aim of this research is to study how cyclones interact with the thinning sea ice
- ERA5, ERA-Interim (ERA-I), Climate Forecast System Reanalysis (CFSR) and satellite data from NSIDC are used together with a cyclone tracking algorithm by Alex Crawford and Mark Serreze (Crawford, 2017) to gain insight on the relationships between Arctic cyclones and sea ice.
- Among other metrics, ACE is used to measure cyclone intensity. The ACE metrics used are based on the squared average wind speed over the cyclone area (ACEarea) and on the squared maximum wind speed in the cyclone area (ACEmax).
- Results are divided into cold (December-May) and warm season (June-November).

Results

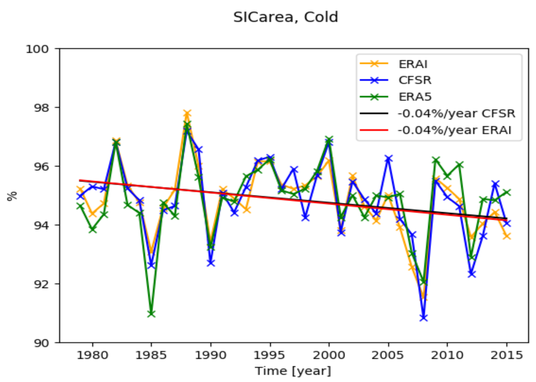

Figure 1: Sea ice concentration timeseries

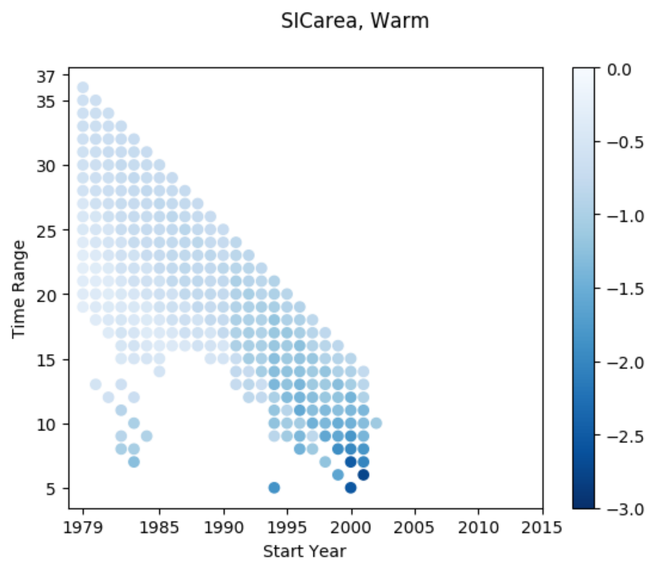

Figure 2: Warm season sea ice concentration trend

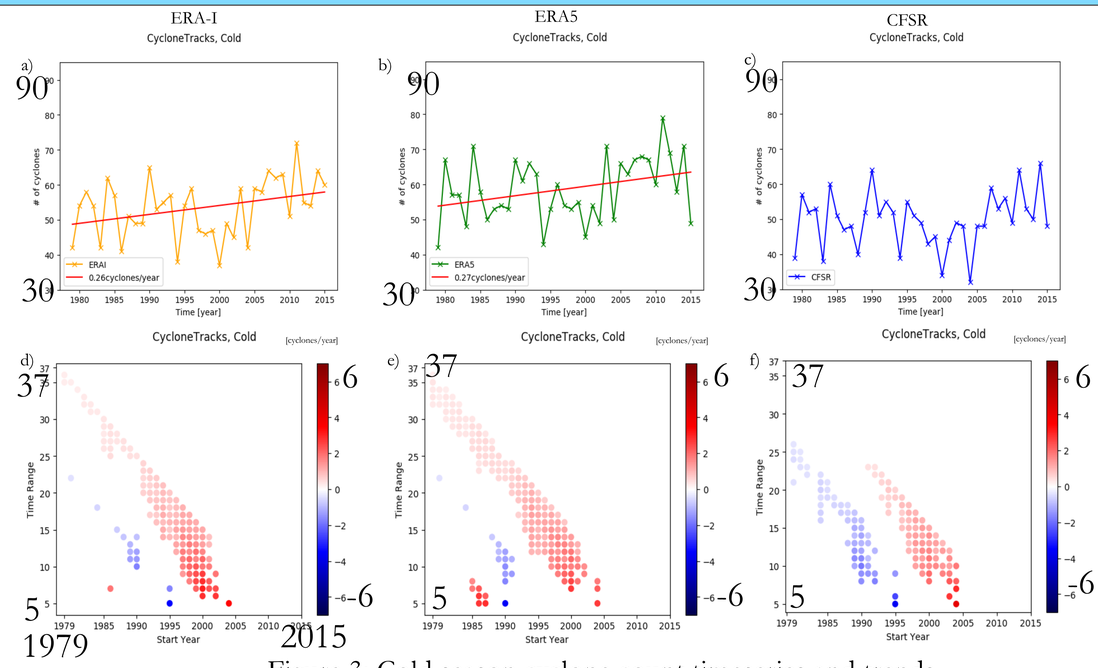

Figure 3: Cold season cyclone count timeseries and trends

SIC	Cyclone Tracks - Cold			SIC	Cyclone Tracks - Warm		
	ERA-I	ERA5	CFSR		ERA-I	ERA5	CFSR
COLD	**-0.45**	**-0.30**	-0.25	COLD (Preceding)	0.03	-0.07	-0.08
WARM (Following)	**-0.55**	**-0.47**	**-0.41**	WARM	0.08	0.16	-0.01

Table 1: Correlation between cyclone counts and SIC

SIC	COLD - intensity						SIC	WARM - intensity					
	ACEmax			ACEarea				ACEmax			ACEarea		
	ERA-I	ERA5	CFSR	ERA-I	ERA5	CFSR		ERAI	ERA5	CFSR	ERA-I	ERA5	CFSR
COLD	-0.20	**-0.41**	**-0.34**	**-0.31**	**-0.39**	-0.26	COLD (Preceding)	0.02	-0.14	-0.14	0.00	-0.14	-0.08
WARM (Following)	-0.05	0.12	0.17	-0.05	0.12	0.26	WARM	0.15	0.06	-0.32	0.19	0.10	-0.08

Table 2: Correlation between cyclone intensity (ACE) and SIC

Key Conclusions

- An increasing trend is observed in the cold season cyclone counts in the late 1990s early 2000s (**Fig. 3**) at the same time as SIC experienced strong decreasing trend in both seasons (**Fig. 1,2**)
- Less sea ice is related to more Arctic cyclones, this is especially true if the cyclone counts precede SIC (**Table 1**)
- Less sea ice is also associated with stronger cyclones, but only for cold season (**Table 2**)

Contact: elina.valkonen@colorado.edu

References

- Crawford, A, 2017: The influence of the Arctic frontal zone on summer cyclone activity today and in the future. Ph.D thesis, Dept. of Geography, U of Colorado, 217pp.

The detection of Arctic Sea Ice Leads in the offshore Alaska, Beaufort Sea Region.

UTSA The University of Texas at San Antonio™

Jullian C.B. Williams, Dr. Hongjie Xie, Dr. Alberto M. Mestas-Nuñez, Dr. Stephen Ackley

NASA Center for Advanced Measurements in Extreme Environments (CAMEE), The University of Texas at San Antonio, TX, USA

Introduction

Objectives

1. Detect lead fractions:
   - Open water
   - Thin ice
2. Validate detected lead areas.
3. Perform time series analysis with lead geometry properties.
   - Orientation.
   - Lead width.
   - Lead length.
   - Distribution.

Study area

Figure 1 shows the study area in the offshore Alaska - Beaufort sea region.

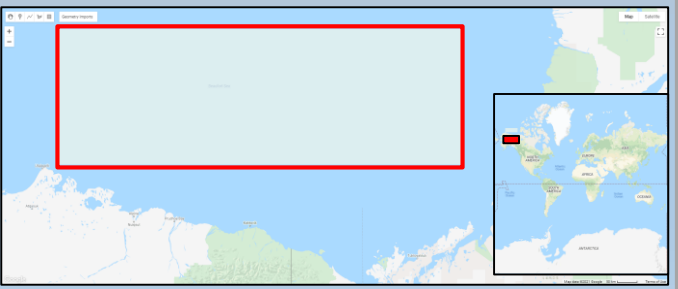

Figure 1: Offshore Alaskan region. ~ 300 m into Beaufort Sea area.

Data and Method

Data

1. Sentinel-1 Synthetic Aperture Radar (SAR).
2. Sentinel-2 Multi-Spectral Instrument (MSI).
3. IceSat-2 Laser Altimeter.

Methods

1. Sentinel-1 SAR image correction.
2. Sentinel-2 true color composite cloud removal.
3. Supervised machine learning of Lead objects.
   - Image Segmentation.
   - Surface Roughness.
   - Support Vector Machine (SVM).
   - Total freeboard of ridge vs. lead areas.
4. Vector analysis.

Results and Discussion

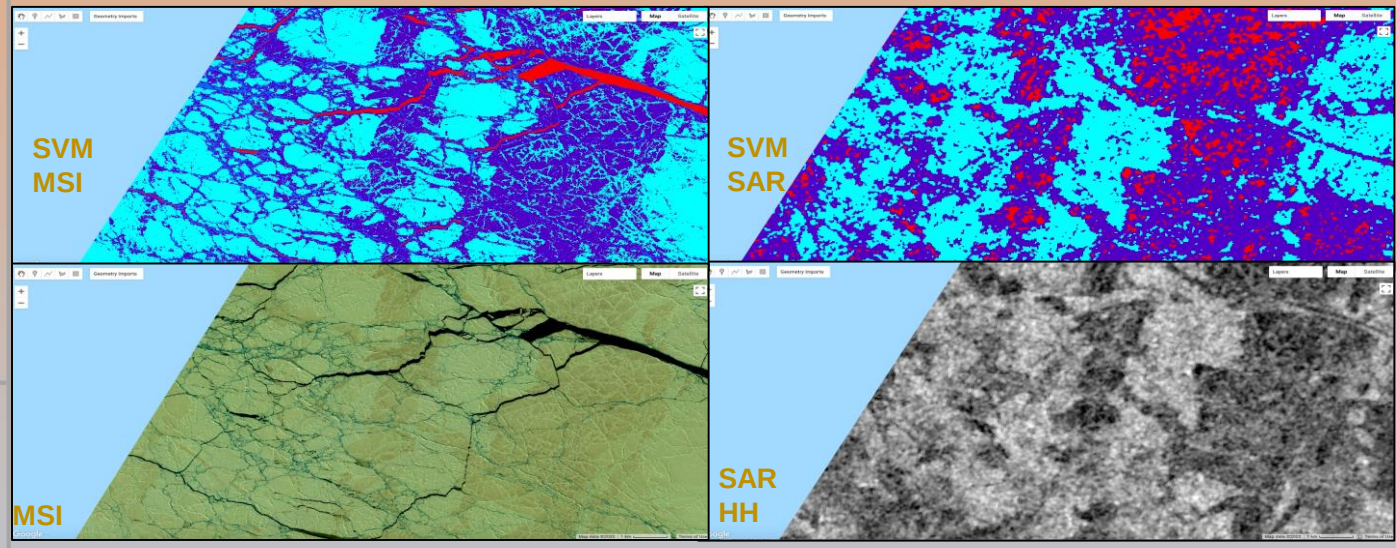

Figure 2: Left: Sentinel-2 (band 4-3-2) (bottom) and classified output (top). Right: Sentinel-1 (HH) (bottom) and classified output (top). SVM – support vector machine.

Date: Apr 29,2019

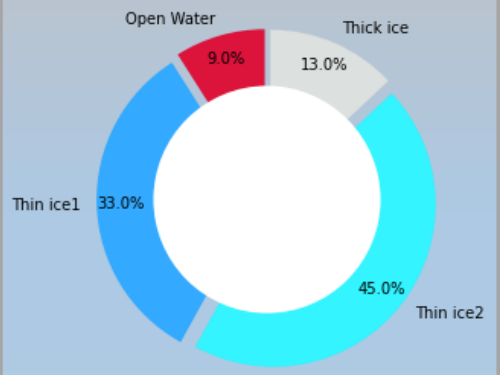

Graph 1: Lead fraction output from SVM-SAR-HH output.

Date: Apr 29,2019

- Net lead orientation is typically towards the East. (towards Bank's island and Canadian archipelago).
- Classification accuracy = 91%.
- Detected leads are segmented. Improvement on segmentation is needed.
- Ice ridges can be separated from leads using total freeboard.
- Use of a convolution neural network (CNN) can improve class accuracy and lead geometry segments.